Title

Cadherins can dimerize via asymmetric interactions

Journal

FEBS Letters, 596(13)

ISSN

0014-5793

Authors

Priest, Andrew Vae
Koirala, Ramesh
Sivasankar, Sanjeevi

Publication Date

2022-07-01

DOI

10.1002/1873-3468.14373

Peer reviewed

Published in final edited form as:

FEBS Lett. 2022 July ; 596(13): 1639–1646. doi:10.1002/1873-3468.14373.

Cadherins can dimerize via asymmetric interactions

Andrew Vae Priest[#],

Ramesh Koirala[#],

Sanjeevi Sivasankar[*]

Department of Biomedical Engineering, University of California, Davis, CA 95616

Abstract

Cadherins are essential cell-cell adhesion proteins that interact in two distinct conformations: X-dimers and strand-swap dimers. Both X-dimers and strand-swap dimers are thought to exclusively rely on symmetric sets of interactions between key amino acids on both cadherin binding partners. Here, we use single-molecule Atomic Force Microscopy (AFM) and computer simulations to show that symmetry in cadherin binding is dispensable and that cadherins can also interact in a novel conformation that asymmetrically incorporates key elements of both strand-swap dimers and X-dimers. Our results clarify the biophysical rules for cadherin binding and demonstrate that cadherins interact in a more diverse range of conformations than previously understood.

Keywords

classical cadherins; cell adhesion; conformation; *trans* interactions; strand-swap dimer; X-dimer; AFM force measurements; single molecule; molecular dynamics

INTRODUCTION

E-cadherin (Ecad) is a prototypic classical cadherin which maintains the physical connection between epithelial cells and plays key roles in tissue morphogenesis and wound healing. Ecad adhesion is carefully regulated to orchestrate complex movement of cells and dysregulation of adhesion is a characteristic of certain cancers (1).

[*]CORRESPONDING AUTHOR: ssivasankar@ucdavis.edu.

[#]Equal contribution

Author contributions:

A.V.P., R.K. and S.S. designed research; S.S. directed the research; A.V.P. and R.K. performed AFM experiments; A.V.P. performed computer simulations; A.V.P., R.K. and S.S. wrote the paper.

Declaration of Interests: The authors declare no competing interests.

Ecads from opposing cells bind via two distinct calcium dependent conformations, with different adhesive strengths: strand-swap dimers and X-dimers (2, 3). These distinct dimer structures are formed by symmetric interactions, i.e., both interacting Ecads contribute equally to bond formation using mirror interactions between key amino acids. Strand-swap dimers, which are the more robust binding conformation, are formed by the symmetric exchange of Tryptophan-2 (W2) residues between interacting Ecads (4). In contrast, X-dimers are primarily formed by symmetric pairs of salt-bridges between Lysines (K14s) and Aspartic acids (D138s) on both Ecads (5, 6).

Cells regulate Ecad adhesion by switching between X-dimers and strand-swap dimers (7). Ecad ectodomains are believed to initially form X-dimers and then transition to strand-swap dimers through an intermediate conformation that resembles an X-dimer, but with both W2 residues swapped (Figure 1a) (6, 8, 9). Mutating both W2 and K14 abolishes the ability of Ecad monomers to interact homophilically and form *trans* dimers (6). Consequently, dual-mutated Ecad constructs are extensively used as controls to abrogate adhesion (10–13). However, the possibility that Ecads can form *trans* dimers without the symmetric involvement of two W2s or of two K14-D138 salt-bridges, from both binding partners, has never been investigated.

Here we perform single-molecule force measurements using an atomic force microscope (AFM) with a range of Ecad mutants and directly show that wild type Ecad can interact with dual-mutated Ecad lacking both X-dimer and strand-swap dimer interfaces. Using protein structure prediction and molecular dynamics simulations, we show that wild type and dual-mutated Ecads interact in a novel conformation, by asymmetrically swapping one W2, while simultaneously forming one K14-D138 salt bridge.

MATERIALS AND METHODS

Purification of Ecad ectodomain.

Wild type and mutant Ecad ectodomains were generated using plasmids containing a C-terminal AviTag sequence as described previously (14). The plasmids were incorporated into pcDNA3.1(+) vectors and were transiently transfected into HEK 293T cells using PEI (Millipore Sigma) (15). Three to four days post transfection, conditioned media was collected for protein purification. Conditioned media containing his-tagged Ecads was passed through a chromatography column containing Ni-NTA agarose beads (Qiagen). Beads were then washed with biotinylation buffer (25mM HEPES, 5mM NaCl, and 1mM $CaCl_2$; pH 7.5). Ecads bound to the Ni-NTA beads were biotinylated with BirA enzyme (BirA 500 kit; Avidity) for 1hr at 30°C. The free biotins were subsequently removed from the Ni-NTA column and biotinylated Ecads bound to Ni-NTA beads were eluted using a buffer containing 200mM Imidazole, 20mM Na_2HPO_4, 500mM NaCl, and 1mM $CaCl_2$ (pH 7.5). Presence of Ecad was verified with SDS-PAGE and concentration was quantified by measuring absorbance at 280nm (Quickdrop, Molecular Devices). Typically, ~450ml of conditioned media yielded ~250–300 μg of purified Ecad. Biotinylation efficiencies of different Ecad mutants were compared by western blotting using Streptavidin Alexa Fluor 647 conjugate (catalog no. S21374; Life Technologies) and detected using the ChemiDoc system from BioRad.

Ecad functionalization on glass coverslips and AFM cantilever.

Immobilization of purified Ecad ectodomains on glass coverslips (CS) and Si tip of AFM cantilevers (Hydra 2R-50N; AppNano) has been described previously (9, 11, 13, 14). Briefly, the CS and cantilevers were cleaned by immersing in 25% H_2O_2/75% H_2SO_4 solution overnight and washed with deionized water. The CS were then soaked in 1M KOH and washed with deionized water. Both the CS and cantilevers were then washed with acetone and were functionalized with amine groups by immersing in 2% (vol/vol) 3-aminopropyltriethoxysilane (Millipore Sigma) solution dissolved in acetone. Polyethylene glycol (PEG) (MW 5000, Lysan Bio) spacers containing an amine-reactive N-hydroxylsuccinimide ester group at one end were covalently attached to the cantilever (100 mg/ml in 100 mM $NaHCO_3$ dissolved in 600mM K_2SO_4, for 4 hrs); 10% of the PEG spacers presented biotin molecules at the other end. PEG-functionalized CS and cantilevers were incubated in 1 mg/ml Bovine Serum Albumin (13) overnight. The CS and cantilevers were then sequentially incubated with streptavidin (0.1 mg/ml for 30 mins) and biotinylated Ecads (200 nM for 45 mins); the incubation concentration for K14E was 600 nM since only a third of the protein was biotinylated. Finally, free biotin-binding sites of streptavidin were blocked using 80μM free biotin for 20 mins.

AFM force measurements.

Force measurements were performed using an Agilent 5500 AFM with a closed loop scanner. An Ecad-functionalized AFM cantilever was brought into contact with an Ecad-functionalized CS and held for 0.1s before the cantilever was retracted at one of six constant velocities (0.23, 0.43, 1.0, 2.8, 5.3, 10 μm/s) (Figure 1b). All the experiments were performed in pH 7.4 buffer solution containing 10 mM Tris-HCl, 100 mM NaCl, 10 mM KCl and 8 μM free biotin with either 2.5 mM $CaCl_2$ or 2.5 mM EGTA. A typical experiment consisted of measurement of ~12150 force-distance traces in Ca^{2+} followed by ~6500 force-distance traces in EGTA. Cantilever spring constants were measured using the thermal fluctuation method (16).

Analysis of AFM data.

Force-distance traces were initially separated into two categories using a convolutional neural network model: those containing rupture events (including nonspecific and multiple unbinding events) and those without any unbinding events. Force-distance traces containing rupture events were further categorized using custom MATLAB scripts. Single unbinding events with characteristic PEG stretching were accepted as specific Ecad-Ecad interactions. In order to minimize the probability of accepting rupture events arising from nonspecific interaction of protein with the opposing surface (resulting in single PEG stretching), we rejected force curves with contour lengths ≤ 30 nm since this corresponds to a single PEG being stretched. The contour lengths of PEG tethers were determined by fitting the PEG stretching region of each rupture force curve to a worm-like chain (WLC) model (17) using nonlinear least squares fitting. Unbinding forces greater than 75 pN were rejected since the probability of biotin-streptavidin rupture increases with increasing force; this represented a loss of < 7% of the data. Finally, we filtered the data based on the root mean square error of the WLC fits. Only root mean squared errors that were less than the mean plus one

standard deviation were retained. Loading rates were calculated as described previously (18) and grouped using K-means clustering algorithm, as described previously (19). Forces and loading rates were bootstrapped and clustered. Median forces and median loading rates were calculated for each bootstrap group and fit to the Bell-Evans model (20, 21) using nonlinear least squares fitting with bisquare weight. We determined the values of the dissociation rate in the absence of force (k_{off}) and width of the confining energy barrier (x_β) from the median of the bootstrap fits. Uncertainties in k_{off} and x_β were calculated as the median absolute deviations.

AlphaFold and molecular dynamics simulations.

The WT-Dblm structure was predicted using AlphaFold-Multimer installed locally from the github repository (https://github.com/deepmind/alphafold). The sequence of mouse Ecad EC1–2 (residues 1–213) was used for the wild type Ecad and the double mutant input was the same sequence with two point mutations W2A and K14E introduced. We used the default parameters and selected the top-ranked structure according to the pLDDT score (ranked_0.pdb) for all subsequent molecular dynamics simulations of WT-Dblm. Molecular dynamics simulations (using the AlphaFold WT-Dblm structure and PDB structures: 2QVF, 3LNH, 3LNE) were setup and performed using Gromacs as described previously (7). The stability of each dimer was monitored by calculating the root mean squared deviation (RMSD) of the dimer relative to the initial structure. RMSDs were calculated from the MD trajectory files using *gmx rms* in Gromacs. Distances were calculated using the built-in Gromacs command *gmx paridist*. Hydrogen bonds were classified using the built in Gromacs command *gmx hbond* based on the geometric criteria that the distance between the donor and accepter was less than or equal to 0.35 nm and the Hydrogen-Donor-Acceptor angle was less than or equal to 30 degrees.

Statistical analysis.

Tests of statistical significance between event rates were performed using Chi-squared tests of independence with Yates' correction on 2×2 contingency tables of specific events and nonspecific events comparing two conditions. Center of mass distances were statistically compared using unpaired t-tests without assuming the data comes from distributions with equal variances (otherwise known as Welch's t-test).

RESULTS

Ecad forms asymmetric dimers.

We utilized single-molecule AFM binding assays to determine the relative roles of the strand-swap dimer interface and the X-dimer interface in Ecad binding. We performed experiments using the following Ecad ectodomain constructs: ***WT*** **-** wild type Ecad containing both W2 and K14 residues, ***K14E*** **-** Ecad mutant that cannot form an X-dimer and is trapped in a strand swap dimer conformation (6), ***W2A*** **-** Ecad mutant that cannot form a strand-swap dimer and is trapped in an X-dimer structure (6, 22), and ***Dblm*** **-** Ecad double mutant which incorporates both W2A and K14E mutations and does not bind homophilically (6, 11).

As described previously (14), we immobilized identical concentrations of Ecad ectodomains that were biotinylated at their C-termini, onto AFM cantilevers and glass coverslips functionalized with polyethylene glycol (PEG) linkers and streptavidin (Figure 1b; Materials and Methods). The Ecads on the AFM tip and substrate were allowed to interact before the cantilever was retracted at a constant velocity. Single Ecad interactions were identified from unbinding events preceded by a characteristic nonlinear stretching of the PEG tether (Figure 1c; Materials and Methods). Stretching of PEG was fit to a worm like chain model, which served as a molecular fingerprint for single-molecule unbinding events (Figure 1c; Materials and Methods). To maximize the likelihood of measuring single-molecule interactions, surface density of Ecad was tuned such that the observed binding probability was ~6% (Figure 1d). Poisson statistics predicts that under these conditions, >97% of the observed events correspond to the unbinding of a single Ecad-Ecad bond. Since Ecad-Ecad interactions are calcium dependent, we performed thousands of AFM measurements, with every Ecad mutant, in the presence of either calcium or EGTA—a calcium chelator.

We first confirmed that WT-Ecad was functional by measuring the interactions of WT-Ecad immobilized on both the AFM tip and the substrate in the presence of calcium and EGTA (WT-WT). As expected, our measurements showed that WT-WT binding was calcium dependent ($p = 8.6\times10^{-44}$, Figure 1d). We also confirmed that Ecad binding was abolished when both W2 and K14 were mutated on both binding partners, by performing AFM measurements with the Dblm immobilized on both the AFM tip and substrate (Figure 1d; Dblm-Dblm). As demonstrated previously (11), the low Dblm-Dblm event rate in EGTA established the non-specific binding levels in our experiments.

It is interesting to note that Dblm-Dblm AFM measurements yielded higher binding rates in the presence of EGTA compared to calcium (Figure 1d). While the mechanism by which this occurs is unclear, it has also been observed with other members of the cadherin family of proteins (13, 23). Nonetheless, since Dblm-Dblm does not bind in the canonical conformations (strand-swap and X-dimers), we used the binding rate in EGTA as a proxy for nonspecific interactions in our experiments.

Since the Dblm lacks both the X- and strand-swap binding interfaces, we proceeded to ask if Dblm could interact with opposing W2A, K14E and WT-Ecads. Our measurements showed that while opposing W2A mutants (W2A-W2A) interact to form calcium dependent X-dimers ($p = 3.5\times10^{-20}$), the binding of W2A with Dblm (W2A-Dblm) was lesser than nonspecific adhesion demonstrating that W2A cannot interact with Dblm (Figure 1d). Similarly, our data showed that unlike opposing K14E mutants (K14E-K14E) which form calcium dependent strand-swap dimers ($p = 3.1\times10^{-13}$), the binding of K14E with Dblm (K14E-Dblm) had a low interaction rate (Figure 1d). In contrast, much to our surprise, we measured significant calcium-dependent binding between WT-Ecad and Dblm (WT-Dblm; $p = 1.2\times10^{-34}$), demonstrating that both W2 and K14 are simultaneously needed on Ecad to facilitate its asymmetric adhesion with Dblm (Figure 1d).

WT-Dblm is weaker than strand-swap dimers but comparable to X-dimers.

Since strand-swap dimers have a higher affinity and are the stronger binding conformation compared to X-dimers (6, 7), we measured the force-independent dissociation constants

of interacting Ecad dimers using single-molecule dynamic force spectroscopy (DFS). We measured unbinding forces at different loading rates and analyzed the data using the Bell-Evans model which relates the unbinding force to the natural logarithm of the loading rate (20, 21) (Materials and Methods). This analysis allowed us to estimate the dissociation rate under stress-free conditions (k_{off}) and width of the confining energy barrier (x_β). Since k_{off} is inversely related to the bond lifetime in the absence of force, a lower value of k_{off} represents more stable binding.

Consistent with strand-swap dimers being more stable compared to X-dimers, we found that the k_{off} for WT-WT was significantly lower than W2A-W2A (Figure 2a, c). This corresponded to an unstressed bond lifetime of the WT-WT dimer that was nearly 5 times longer compared to the W2A-W2A dimer. In contrast, the off rate for K14E-K14E dimers was closer to WT-WT (2 times higher; Figure 2b). Finally, despite binding asymmetrically, the k_{off} for WT-Dblm was comparable to the X-dimers formed by W2A-W2A (Figure 2d).

WT-Dblm complex incorporates key elements of strand-swap dimers and X-dimers.

To gain insight into the structure of the WT-Dblm complex, we predicted its structure using AlphaFold-Multimer, a protein prediction tool trained specifically for multimeric inputs of known stoichiometry (24, 25). Since only the two outer domains of the extracellular region (EC1 and EC2) are involved in adhesion, we used AlphaFold-Multimer to predict the structure of EC1–2 WT-Dblm complex (Materials and Methods). A qualitative analysis of the predicted structure showed that while W2 from WT-Ecad was inserted into its binding pocket on Dblm, the mutated A2 on the Dblm was not inserted into the WT-Ecad binding pocket. Simultaneous, one X-dimer salt bridge was formed between K14 of the WT-Ecad and D138 on the Dblm. Not surprisingly, the negatively charged E14 on Dblm, did not form a salt bridge with D138 on WT-Ecad.

Next, to ensure that these asymmetric bonds were stable, we performed MD simulations on the predicted WT-Dblm structure and compared them to identical MD simulations performed on crystal structures for WT-WT (PDB ID: 2QVF), K14E-K14E (PDB ID: 3LNE) and W2A-W2A (PDB ID: 3LNH) (Materials and Methods). Five MD simulations were performed on each dimer structure, and root mean squared deviations (RMSDs) were calculated. The RMSDs of the MD trajectories showed that all structures equilibrated within 20 ns (Figure S1).

To compare strand-swap interactions we aligned the WT-WT, K14E-K14E, and WT-Dblm structures from the end of each MD simulations (Figure 3a). While the WT-Dblm did not resemble a strand-swap dimer, when we aligned the structures based on the W2 binding pocket (residues 26–28, 36, 78–80, 89–92), the W2 residues from all three structures aligned almost perfectly (Figure 3b). The distance between the centers of mass of each W2 and its binding pocket throughout the MD simulations were similar for the two W2s in the WT-WT and K14E-K14E structures and for the single W2 in the WT-Dblm structure (Figure 3c). In contrast, the mutated A2 in the WT-Dblm structure was not inserted into its binding pocket (Figure 3c). These results showed that the WT-Dblm formed the same strand-swap interaction as WT-WT and K14E-K14E, albeit from only one Ecad instead of both Ecads.

Next, we performed a comparison of X-dimer interactions between the WT-Dblm structure and the W2A-W2A X-dimer structure. Structural alignment showed significant similarities between both structures (Figure 3d) with identical salt bridge K14:D138 interactions (Figure 3d). When we compared the distance between K14 and D138 throughout the MD simulation, we observed that the distances between K14 and D138 for both salt-bridges in W2A-W2A and for the one salt-bridge in WT-Dblm were similar (Figure 3f). In contrast, the E14 mutation in the Dblm, did not form a salt bridge with the D138 from the opposing WT-Ecad (Figure 3f).

Taken together, this structural analysis showed that WT-Dblm binds in a conformation that resembles an X-dimer, albeit with a swapped W2 residue. However, the interactions in WT-Dblm are asymmetric with only one strand-swapped W2 and one K14:D138 salt bridge.

DISCUSSION

Our AFM binding assays show that Ecad can form asymmetric homophilic dimers and that an asymmetric bond requires two binding interfaces: one asymmetric X- and one asymmetric strand-swap interface (Figure 1d). DFS analysis shows that the k_{off} of WT-Dblm is comparable to W2A-W2A if not slightly lower which implies that the WT-Dblm may be more stable than an X-dimer, while both WT-Dblm and W2A-W2A dimers are less stable than the symmetric strand-swap dimers WT-WT and K14E-K14E (Figure 2). Structure prediction and molecular dynamics simulations show that WT-Dblm binds in a conformation which resembles an X-dimer, but with one asymmetric salt-bridge and one asymmetrically swapped W2 (Figure 3). In addition to binding in a *trans* conformation, neighboring Ecad also form *cis* dimers (26). However, the WT-Dblm interactions are not due to *cis* dimer formation since we do not see significant binding between K14E-Dblm, W2A-Dblm, or Dblm-Dblm in our AFM assays.

While both the WT-WT dimer and the K14E-K14E dimer exist as strand-swap dimers, our DFS analysis demonstrates that the K14E-K14E interaction is slightly weaker than WT-WT (WT-WT $k_{off} = 0.37\ s^{-1}$; K14E-K14E $k_{off} = 0.78\ s^{-1}$). This finding is partially explained by looking at the hydrogen bonds that are formed between Ecads in the MD simulations. We observed eight stable hydrogen bonds that existed consistently throughout the MD trajectory for WT-WT, but only seven such bonds for K14E-K14E (Figure S2a, b). Notably, one of the seven bonds in K14E-K14E did not occur consistently across all 5 MD simulations (25LYS:3VAL; Figure S2b). This suggests that subtle differences in intermolecular interactions may lead to the K14E-K14E dimer being slightly weaker than WT-WT. Perhaps expectedly, the WT-Dblm dimer shows key strand-swap interactions TRP2:90ASP and 3VAL:25LYS, as well as key X-dimer interactions 14LYS:138ASP and 101GLN:100ASP (Figure S2). This analysis reinforces our finding that two adhesive interfaces (one strand-swap and one X-dimer interface) are necessary for asymmetric adhesion.

It is likely that the asymmetric interaction observed with WT-Dblm corresponds to an intermediate step along the pathway for formation of strand-swap dimers. Previously, using MD simulations, we uncovered a putative Ecad binding intermediate that resembles an

X-dimer but with two swapped W2 residues (9). Comparing this intermediate conformation to the WT-Dblm dimer shows considerable similarities, particularly for the outermost EC1 domain (Figure S3). Based on the canonical dimerization pathway of Ecad, this suggests that Ecads may form strand-swap dimers by converting from X-dimers into the putative intermediate state via the asymmetric dimer conformation.

Besides providing biophysical insights into the mechanistic basis of cadherin adhesion, our results caution against using the cadherin double mutant as a 'negative' control in monitoring Ecad adhesion. Furthermore, the implications of our results extend beyond cadherin adhesion since they suggest that other proteins that oligomerize homophilically, may also be capable of binding asymmetrically.

Supplementary Material

Refer to Web version on PubMed Central for supplementary material.

Acknowledgments:

This research was supported by the National Institute of General Medical Sciences of the National Institutes of Health (R01GM121885 and R01GM133880). We thank Dr. Shrabasti Bhattacharya for purifying the K14E and WT Ecad constructs used in this work.

Data availability:

All data produced by this research are made available in the manuscript and Supporting Information.

References

1. Mendonsa AM, Na T-Y, Gumbiner BM. E-cadherin in contact inhibition and cancer. Oncogene. 2018;37(35):4769–80. [PubMed: 29780167]
2. Brasch J, Harrison OJ, Honig B, Shapiro L. Thinking outside the cell: how cadherins drive adhesion. Trends Cell Biol. 2012;22(6):299–310. [PubMed: 22555008]
3. Priest AV, Koirala R, Sivasankar S. Single molecule studies of classical and desmosomal cadherin adhesion. Current Opinion in Biomedical Engineering. 2019;12:43–50. [PubMed: 31742239]
4. Boggon TJ, Murray J, Chappuis-Flament S, Wong E, Gumbiner BM, Shapiro L. C-cadherin ectodomain structure and implications for cell adhesion mechanisms. Science. 2002;296(5571):1308–13. [PubMed: 11964443]
5. Pertz O, Bozic D, Koch AW, Fauser C, Brancaccio A, Engel J. A new crystal structure, Ca2+ dependence and mutational analysis reveal molecular details of E-cadherin homoassociation. EMBO J. 1999;18(7):1738–47. [PubMed: 10202138]
6. Harrison OJ, Bahna F, Katsamba PS, Jin X, Brasch J, Vendome J, et al. Two-step adhesive binding by classical cadherins. Nat Struct Mol Biol. 2010;17(3):348–57. [PubMed: 20190754]
7. Koirala R, Priest AV, Yen C-F, Cheah JS, Pannekoek W-J, Gloerich M, et al. Inside-out regulation of E-cadherin conformation and adhesion. Proc Natl Acad Sci U S A. 2021;118(30):e2104090118.
8. Li Y, Altorelli NL, Bahna F, Honig B, Shapiro L, Palmer AG III. Mechanism of E-cadherin dimerization probed by NMR relaxation dispersion. Proc Natl Acad Sci U S A. 2013;110(41):16462–7. [PubMed: 24067646]
9. Manibog K, Sankar K, Kim S-A, Zhang Y, Jernigan RL, Sivasankar S. Molecular determinants of cadherin ideal bond formation: Conformation-dependent unbinding on a multidimensional landscape. Proc Natl Acad Sci U S A. 2016;13(139):E5711–E20

10. Hong SJ, Troyanovsky RB, Troyanovsky SM. Cadherin exits the junction by switching its adhesive bond. J Cell Biol. 2011;192(6):1073–83. [PubMed: 21422232]
11. Rakshit S, Zhang Y, Manibog K, Shafraz O, Sivasankar S. Ideal, catch, and slip bonds in cadherin adhesion. Proc Natl Acad Sci U S A. 2012;109(46):18815–20. [PubMed: 23112161]
12. Wu SK, Yap AS. Patterns in space: coordinating adhesion and actomyosin contractility at E-cadherin junctions. Cell communication & adhesion. 2013;20(6):201–12. [PubMed: 24205985]
13. Shafraz O, Rübsam M, Stahley SN, Caldara AL, Kowalczyk AP, Niessen CM, et al. E-cadherin binds to desmoglein to facilitate desmosome assembly. eLife. 2018;7:e37629.
14. Zhang Y, Sivasankar S, Nelson WJ, Chu S. Resolving cadherin interactions and binding cooperativity at the single molecule level. Proc Natl Acad Sci U S A. 2009;106(1):109–14. [PubMed: 19114658]
15. Longo PA, Kavran JM, Kim M-S, Leahy DJ. Transient mammalian cell transfection with polyethylenimine (PEI). Methods Enzymol. 529: Elsevier; 2013. p. 227–40. [PubMed: 24011049]
16. Hutter JL, Bechhoefer J. Calibration of atomic-force microscope tips. Rev Sci Instrum. 1993;64(7):1868–73.
17. Bustamante C, Marko JF, Siggia ED, Smith S. Entropic elasticity of lambda-phage DNA. Science. 1994;265(5178):1599–600. [PubMed: 8079175]
18. Dudko OK, Hummer G, Szabo A. Theory, analysis, and interpretation of single-molecule force spectroscopy experiments. Proc Natl Acad Sci U S A. 2008;105(41):15755–60. [PubMed: 18852468]
19. Yen C-F, Sivasankar S Improving estimation of kinetic parameters in dynamic force spectroscopy using cluster analysis. J Chem Phys. 2018;148(12):123301.
20. Bell GI. Models for specific adhesion of cells to cells. Science. 1978;200(4342):618–27. [PubMed: 347575]
21. Evans E, Ritchie K. Dynamic strength of molecular adhesion bonds. Biophys J. 1997;72(4):1541–55. [PubMed: 9083660]
22. Sivasankar S, Zhang Y, Nelson WJ, Chu S. Characterizing the initial encounter complex in cadherin adhesion. Structure. 2009;17(8):1075–81. [PubMed: 19646884]
23. Shafraz O, Xie B, Yamada S, Sivasankar S. Mapping transmembrane binding partners for E-cadherin ectodomains. Proc Natl Acad Sci U S A. 2020;117(49):31157–65. [PubMed: 33229577]
24. Jumper J, Evans R, Pritzel A, Green T, Figurnov M, Ronneberger O, et al. Highly accurate protein structure prediction with AlphaFold. Nature. 2021;596(7873):583–9. [PubMed: 34265844]
25. Evans R, O'Neill M, Pritzel A, Antropova N, Senior A, Green T, et al. Protein complex prediction with AlphaFold-Multimer. bioRxiv. 2021:2021.10.04.463034.
26. Harrison OJ, Jin XS, Hong SJ, Bahna F, Ahlsen G, Brasch J, et al. The Extracellular Architecture of Adherens Junctions Revealed by Crystal Structures of Type I Cadherins. Structure. 2011;19(2):244–56. [PubMed: 21300292]

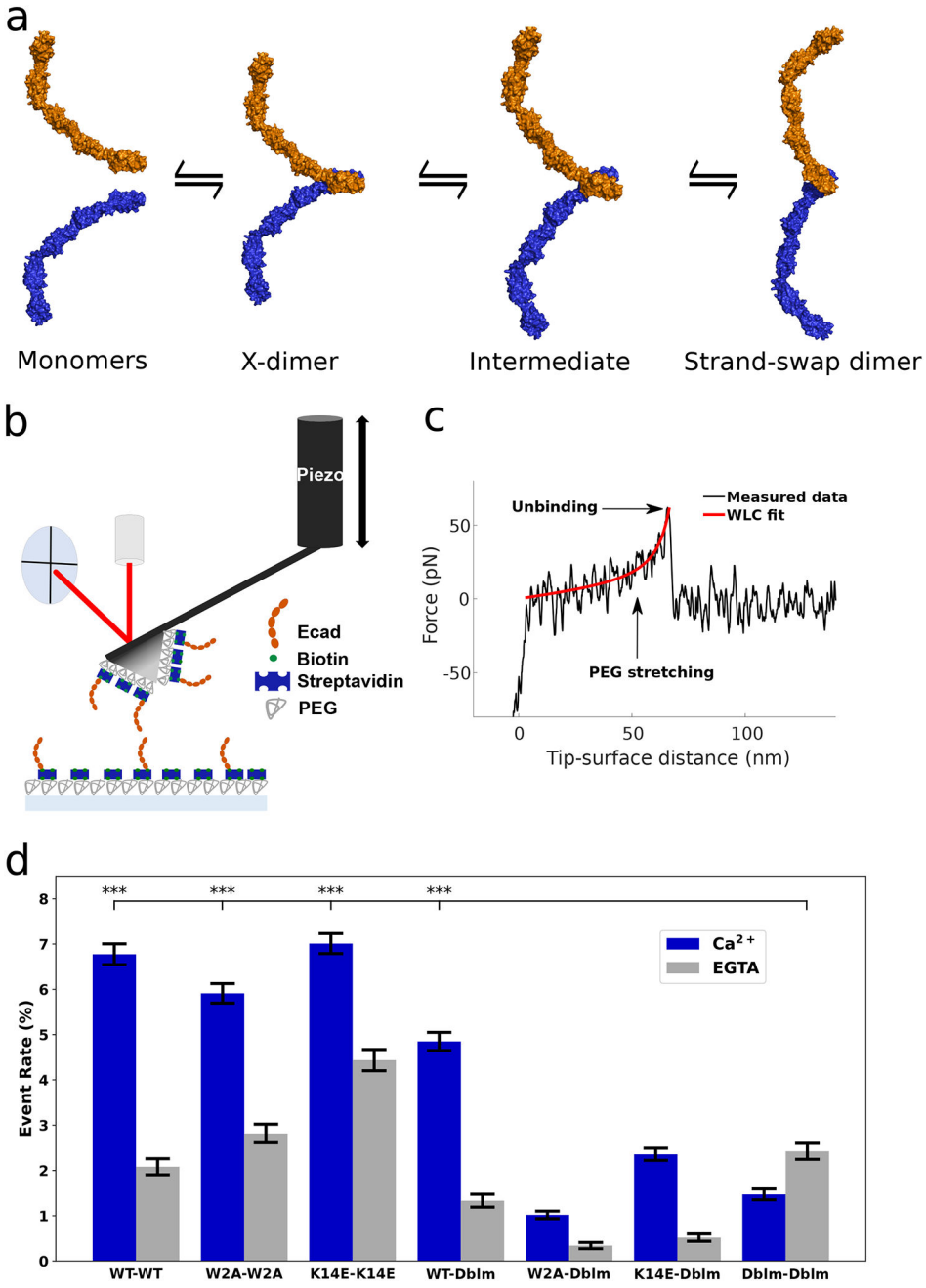

Figure 1. Ecad dimer event rate measured with an Atomic Force Microscope.

(a) Ecad monomers (*left)* interact by first forming an X-dimer (*middle-left*) and transitioning to an intermediate conformation (*middle-right*) before fully converting to a strand-swap dimer (*right*) (strand-swap dimer corresponds to PDB ID: 3Q2V; X-dimer was visualized by alignment to PDB ID: 3LNH; the intermediate conformation was visualized by aligning to the structure found in ref (9)). **(b)** Biotinylated Ecad monomers were immobilized on AFM cantilevers and coverslips functionalized with polyethylene glycol (PEG) and streptavidin. Interactions between Ecad on the cantilever and the coverslip were measured. **(c)** A typical force-distance trace showing single rupture event. PEG stretching region

of the force curve was fit to a worm like chain model (red). **(d)** Binding probabilities were measured using AFM in Ca^{2+} (blue) and EGTA (gray). Total number of Ca^{2+}/EGTA measurements performed for each experiment were 12150/6534 measurements for WT-WT, 12147/6144 measurements for W2A-W2A, 11968/7350 measurements for K14E-K14E, 12150/6534 measurements for WT-Dblm, 12265/7350 measurements for W2A-Dblm, 12394/7350 measurements for K14E-Dblm, and 9654/7350 measurements for Dblm-Dblm. Error bars are the standard deviations of the bootstrapped event rates. Chi-squared tests show significant difference ($p < 0.0001$) between event rates for interacting dimers (WT-WT, K14E-K14E, W2A-W2A, WT-Dblm; in Ca^{2+}) compared to nonspecific interactions (Dblm-Dblm; EGTA). WT-WT:Dblm-Dblm $p = 1.0\times10^{-40}$; K14E-K14E:Dblm-Dblm $p = 1.1\times10^{-43}$; W2A-W2A:Dblm-Dblm $p = 1.5\times10^{-29}$; WT-Dblm:Dblm-Dblm $p = 3.3\times10^{17}$. Chi-squared tests also show that WT-WT, W2A-W2A, K14E-K14E, and WT-Dblm interactions are Ca^{2+} dependent ($p < 0.0001$) with Ca^{2+} *vs.* EGTA p-values of 8.6×10^{-44}, 3.5×10^{-20}, 3.1×10^{-13}, and 1.2×10^{-34} respectively.

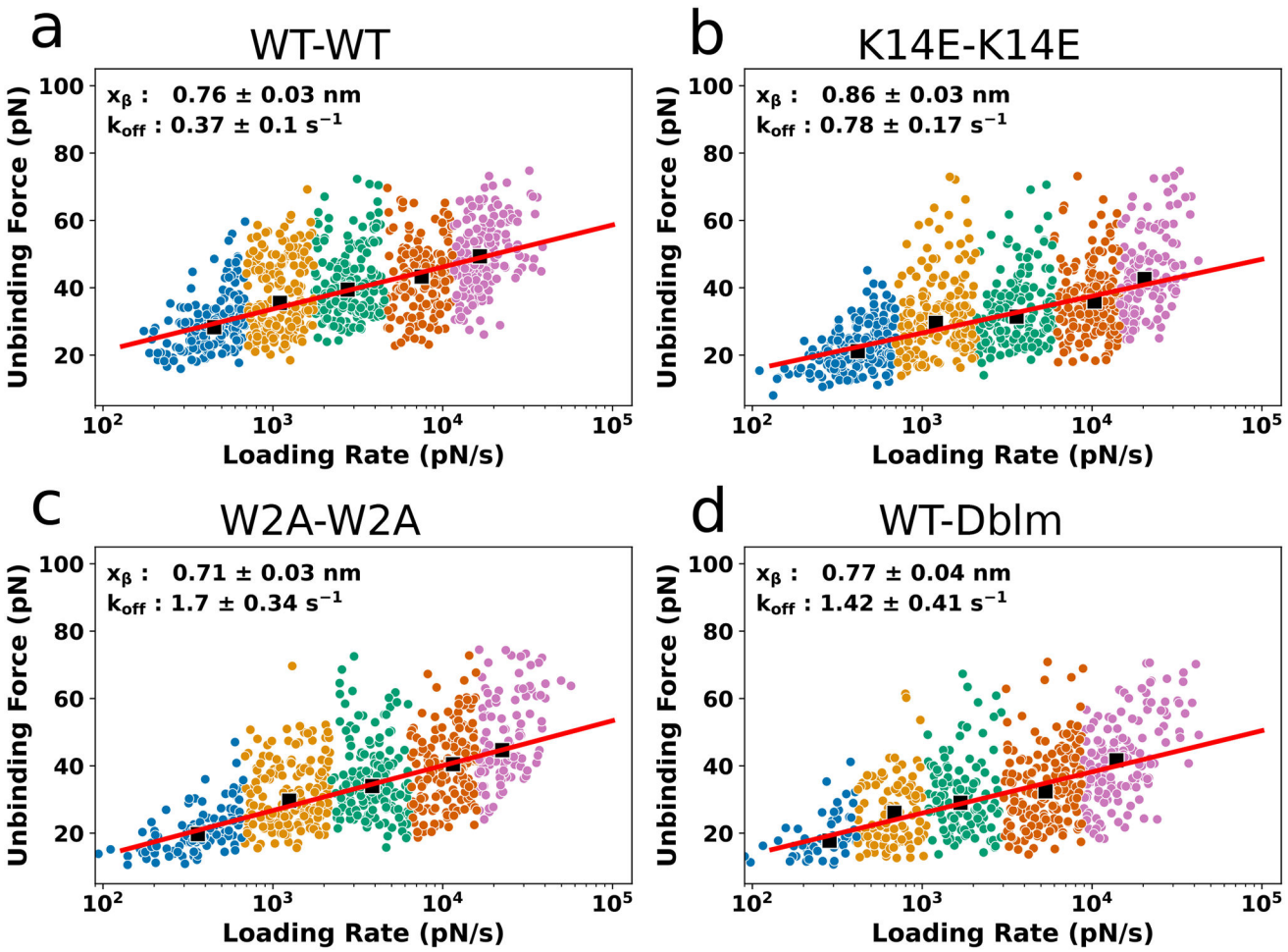

Figure 2. Dynamic force spectroscopy analysis of interacting Ecad dimers.

Loading rates measured in Ca^{2+} for **a)** WT-WT, **b)** K14E-K14E, **c)** W2A-W2A, and **d)** WT-Dblm were grouped together using k-means clustering. The Bell-Evans model (red line) was fit to the median unbinding forces and loading rates (black squares). Uncertainties in k_{off} and x_β are median absolute deviations. Each circle represents a single unbinding event, and colors correspond to the data points from the same cluster.

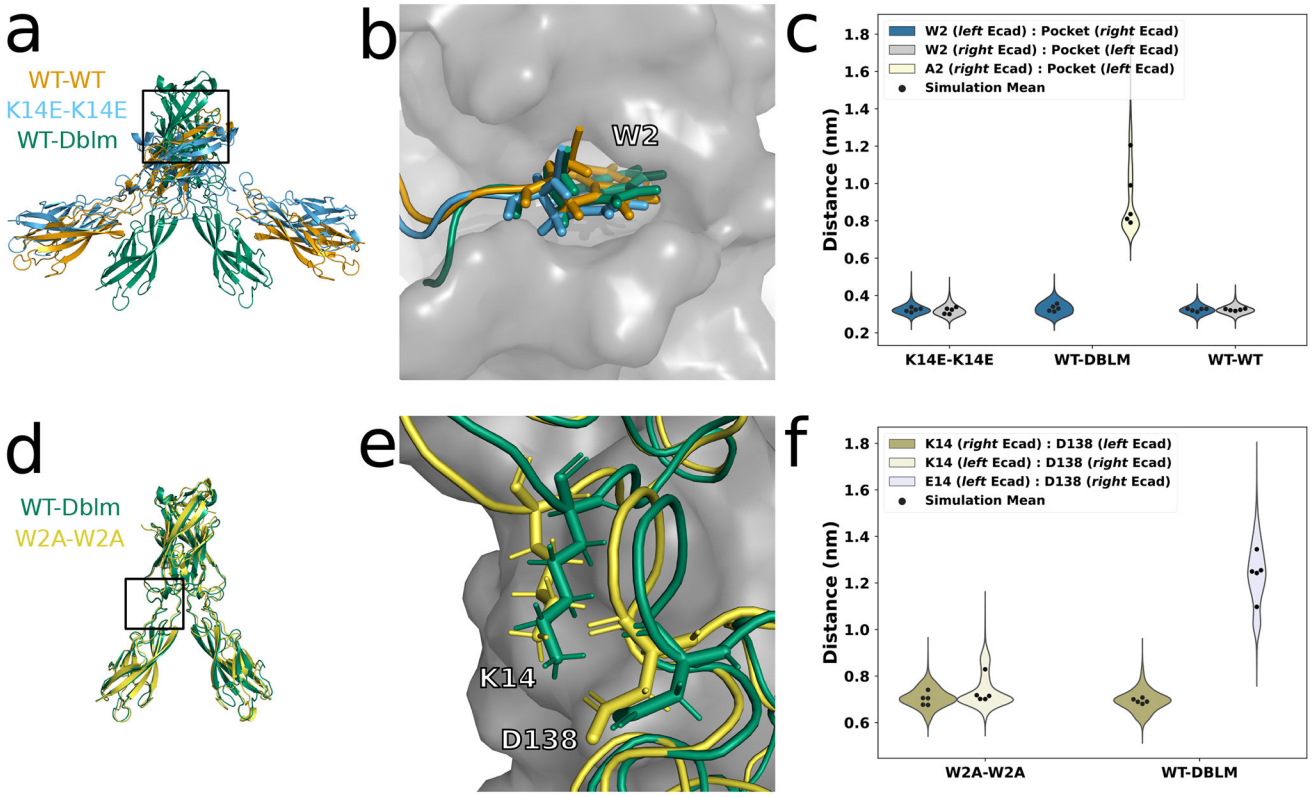

Figure 3: Computational analysis of Ecad dimer structures.

(a) Structural alignment of the final frame of the MD simulations for WT-WT (orange), K14E-K14E (blue), and WT-Dblm (green). **(b)** Close-up of the W2 in the binding pocket of the opposing Ecad (from the black box in panel a). Structures were aligned to each other based on the binding pocket residues. **(c)** Violin plots of the distance between the center of mass of W2 and the respective binding pocket for strand-swap dimers. Distances for the mutated residues of WT-Dblm are also shown. The width of the violin signifies the density of data at that distance. The mean distance from each simulation repeat is overlayed on the violin plots (black circles). **(d)** Structural alignment of the final frame of the MD simulations for W2A-W2A (yellow) and WT-Dblm (green). **(e)** Close-up of the K14:D138 interaction (from the black box in panel d). **(f)** Violin plot of distances between K14 and D138 for X-dimers. The means from each simulation were used to determine the statistical significance between each pair in panels c and f; the distance determined from the mutated residues in WT-Dblm shows significant difference compared to the unmutated residues. Welch's T-test of W2:pocket with W2:pocket had a p-value > 0.1 while W2:pocket with A2:pocket had a p-value ~0.0015. Welch's T-test of K14:D138 with K14:D138 had a p-value > 0.1 while K14:D138 with E14:D138 had a p-value < 0.001. Table of p-values found in (Table S1).